HHS Public Access

Author manuscript

Nature. Author manuscript; available in PMC 2011 March 16.

Published in final edited form as:

Nature. 2010 September 16; 467(7313): 291–296. doi:10.1038/nature09358.

MICU1 encodes a mitochondrial EF hand protein required for Ca^{2+} uptake

Fabiana Perocchi[1], **Vishal M. Gohil**[1], **Hany S. Girgis**[1], **X. Robert Bao**[1], **Janet E. McCombs**[2], **Amy E. Palmer**[2], and **Vamsi K. Mootha**[1]

[1]Center for Human Genetic Research, Massachusetts General Hospital, Boston, MA U.S.A., Broad Institute, Cambridge, MA U.S.A., Department of Systems Biology, Harvard Medical School, Boston, MA U.S.A.

[2]Department of Chemistry and Biochemistry, University of Colorado, Boulder, CO U.S.A.

Abstract

Mitochondrial calcium uptake plays a central role in cell physiology by stimulating ATP production, shaping cytosolic calcium transients, and regulating cell death. The biophysical properties of mitochondrial calcium uptake have been studied in detail, but the underlying proteins remain elusive. Here, we utilize an integrative strategy to predict human genes involved in mitochondrial calcium entry based on clues from comparative physiology, evolutionary genomics, and organelle proteomics. RNA interference against 13 top candidates highlighted one gene that we now call mitochondrial calcium uptake 1 (*MICU1*). Silencing *MICU1* does not disrupt mitochondrial respiration or membrane potential but abolishes mitochondrial calcium entry in intact and permeabilized cells, and attenuates the metabolic coupling between cytosolic calcium transients and activation of matrix dehydrogenases. MICU1 is associated with the organelle's inner membrane and has two canonical EF hands that are essential for its activity, suggesting a role in calcium sensing. MICU1 represents the founding member of a set of proteins required for high capacity mitochondrial calcium entry. Its discovery may lead to the complete molecular characterization of mitochondrial calcium uptake pathways, and offers genetic strategies for understanding their contribution to normal physiology and disease.

The uptake of calcium (Ca^{2+}) by vertebrate mitochondria was first documented nearly 50 years ago[1,2]. These early studies revealed that suspensions of isolated mitochondria can transport and buffer massive amounts of Ca^{2+} across the inner membrane. This high capacity "uniporter" mechanism is classically defined by its dependence on membrane potential, sensitivity to ruthenium red, and activity when extramitochondrial calcium concentrations are in the micromolar range. Subsequent studies, using genetically encoded

---

Correspondence and requests for materials should be addressed to V.K.M. (vamsi@hms.harvard.edu).

Supplementary Information accompanies the paper on www.nature.com/nature.

Competing Interests. The authors declare no competing interests.

Authors' Contributions statement. F.P. and V.K.M conceived of the project and its design. F.P., V.M.G., H.S.G., X.R.B., J.M., and A.E.P. performed experiments and data analysis. F.P. and V.K.M. wrote the manuscript.

calcium indicators targeted to mitochondria3,4,5, were crucial in establishing the physiologic relevance of mitochondrial calcium uptake in a variety of cell types.

It is now widely accepted that mitochondrial Ca^{2+} uptake can shape cytosolic Ca^{2+} signals and oscillations to regulate diverse physiologic processes ranging from hormone secretion to cell differentiation6,7. Mitochondrial Ca^{2+} buffering seems to be particularly important at privileged microdomains near the ER and plasma membrane, where Ca^{2+} concentrations can reach high micromolar levels8. Mitochondrial Ca^{2+} uptake can stimulate TCA cycle dehydrogenases, providing a mechanism of "feed-forward" control whereby Ca^{2+} signals ATP consumptive processes in the cytosol while also stimulating its production in mitochondria9,10,11. Excessive uptake of Ca^{2+}, however, can trigger the permeability transition, leading to cell death and contributing to pathogenesis12.

Although the biophysical properties of mitochondrial Ca^{2+} uptake have been extensively characterized13,14,15, the underlying molecular machinery has remained elusive. Several groups reported the reconstitution of mitochondrial Ca^{2+} uptake activity in *in vitro* systems, yet were unsuccessful in identifying the underlying proteins16,17,18. Since we lack specific, cell-permeant small molecules with which to interrogate these uptake pathways, it is difficult to rigorously evaluate how mitochondrial calcium uptake impacts development and disease15,19 . Furthermore, there are discrepancies between whole cell, isolated mitochondria, and electrophysiological studies of calcium uptake15, and multiple transport mechanisms may exist20, further underscoring the need to identify the underlying molecule machinery. Genetic screens hold the potential to reveal such machinery, as evidenced by the recent identification of an antiporter involved in mitochondrial calcium efflux21.

Here, we report a focused RNAi strategy to identify mitochondrial proteins required for Ca^{2+} uptake based on clues from comparative physiology and organelle proteomics. Key to our approach is the observation that classically defined mitochondrial Ca^{2+} uniporter activity is evolutionarily conserved in vertebrates and in kinetoplastids22,23,24, yet not measurable in the yeast *S. cerevisiae*22,25,26. By searching for inner mitochondrial membrane proteins that share this evolutionary profile, we are able to prioritize a small handful of human proteins that we then test using RNAi. Our strategy has enabled us to spotlight MICU1, a poorly characterized EF-hand containing protein, which we now show is localized to the mitochondrion and required for mitochondrial Ca^{2+} uptake in HeLa cells.

Targeted-RNAi screen

To prioritize proteins required for mitochondrial Ca^{2+} entry, we combined proteomic, physiologic, and evolutionary clues (see Methods). Based on decades of biochemical characterization, we expect the high capacity, ruthenium-red sensitive mitochondrial Ca^{2+} uptake machinery to be (i) localized to mitochondria1,2, (ii) associated with its inner membrane, (iii) expressed in the majority of mammalian tissues22, and (iv) to have homologues in vertebrates22 and kinetoplastids23,24, but not in the yeast *S. cerevisiae*22,25,26. We used a proteomic inventory of 1098 mouse mitochondrial proteins from 14 tissues (called MitoCarta), 1013 of which we previously mapped to human genes27. Of the 1013 human MitoCarta proteins, 18 fulfilled the above criteria as they have also been

reported in purifications of the mitochondrial inner membrane28,29, found in the majority of mammalian organs, and conserved to kinetoplastids but not in yeast27 (Fig. 1a). We prioritized 13 of these 18 genes for which RNAi reagents were available and seemed like plausible candidates.

We performed an RNAi screen of these top 13 candidates in a commercially available HeLa cell line (mt-AEQ) that stably expresses a mitochondria-targeted aequorin3 (see Methods). We used ~ five short hairpin RNA (shRNA) constructs targeting each of the 13 genes and expressed them via lentiviral transduction in biological duplicate (Supplementary Table 1). Histamine stimulation of this reporter cell line leads to an inositol-1,4,5-triphosphate (IP_3)-triggered rise in cytosolic Ca^{2+} that is rapidly buffered by mitochondria, resulting in light emission30. Luminescence from mtAEQ is influenced by $[Ca^{2+}]_m$ as well by the number of viable cells in the population (Supplementary Fig. 1).

We sought to identify hairpins that attenuated mitochondrial Ca^{2+} uptake even after normalizing for cell number. The majority of candidate or control hairpins had no impact on mitochondrial Ca^{2+} uptake or only a secondary effect due to decreased cell number (Fig. 1b). However, one hairpin corresponding to *CBARA1* (accession *FLJ12684*), which we now term mitochondrial calcium uptake 1, a poorly characterized gene, gave rise to a dramatic Ca^{2+} phenotype scoring well outside of this distribution in two independent replicate screens (Fig. 1b). This hairpin (sh1-*MICU1*) drastically reduced mitochondrial Ca^{2+} uptake independent of effects on cell viability. Next, we created four stable mt-AEQ HeLa cell lines in which we silenced the expression of *MICU1* using four distinct hairpins targeting the gene (Fig. 1c). The mitochondrial Ca^{2+} uptake phenotype showed a strong correlation to the strength of *MICU1* knockdown (Fig. 1c). It is notable that silencing of *MICU1* by the two most effective hairpins (sh1 and sh2-*MICU1*, giving 90% and 89% knockdown, respectively) resulted in similar Ca^{2+} phenotypes, although two distinct regions of the transcript had been targeted, suggesting an on-target mechanism of action of these hairpins.

To formally exclude an off-target effect of sh1-*MICU1* on the mitochondrial Ca^{2+} phenotype, we performed a cDNA rescue study in stable sh1-*MICU1* cells. We engineered a hairpin-insensitive cDNA harbouring eight synonymous mutations within the sh1 target sequence and stably expressed it in sh1-*MICU1* cells via lentiviral transduction using orthogonal antibiotic selection (see Methods). As reported in Fig. 1d, expression of the hairpin-insensitive *MICU1* in knockdown cells was sufficient to fully restore mitochondrial Ca^{2+} uptake in sh1-*MICU1* knockdown cells. Gene expression analysis by qPCR revealed that the endogenous *MICU1* expression, which we measure with a 3'-UTR specific gene expression assay, was still silenced, while the exogenous RNAi insensitive transcript was highly expressed (Fig. 1e), demonstrating that the phenotypic rescue is attributable to exogenous expression of *MICU1*. The knockdown:phenotype correlation, combined with the cDNA rescue study firmly establish that the observed RNAi phenotype is attributable to silencing of *MICU1* and not due to an off-target effect.

OXPHOS function in *MICU1*-silenced cells

Because mitochondrial Ca^{2+} uptake is dependent on mitochondrial membrane potential (ψ_m), any defect in the electron transport chain or in membrane polarization could in principle give rise to a secondary defect in Ca^{2+} uptake. We therefore sought to determine whether knockdown of *MICU1* affected ψ_m or respiration in intact cells. ψ_m of *MICU1*-silenced cells was comparable to control cells, and in both cases, could be fully depolarized using the uncoupler carbonyl cyanide m-chlorophenylhydrazone (CCCP) (Fig. 2a). We next tested the impact of *MICU1* knockdown on mitochondrial oxidative phosphorylation, by measuring oxygen consumption rate (OCR) of intact cells at baseline and following treatment with key electron transport chain inhibitors or uncouplers. We found that the basal respiration rate was fully preserved in sh1-*MICU1* knockdown cells (Fig. 2b). Moreover, the ATP-coupled respiratory rate, the maximal uncoupled rate, and the leak rate of respiration were similar in control and sh1-*MICU1* knockdown cells (Fig. 2c). Mitochondrial DNA (mtDNA) copy number was also unchanged (Fig. 2d). Collectively, these data demonstrate that mitochondrial respiratory physiology is intact in *MICU1* silenced cells and that the mitochondrial Ca^{2+} uptake phenotype is not a secondary consequence of generalized dysfunction in this organelle.

Secondary assays of Ca^{2+} homeostasis

We next performed detailed secondary analyses of Ca^{2+} homeostasis in sh1-*MICU1* knockdown cells, using multiple techniques (Fig. 3).

First, we measured mitochondrial Ca^{2+} uptake in populations of cells using two methods to mobilize Ca^{2+}. As can be seen in Fig. 3a, histamine stimulated IP_3-signaling in control mt-AEQ HeLa cells (pLKO.1) resulted in typical kinetics of mitochondrial calcium uptake3. However, mitochondrial Ca^{2+} uptake was impaired by silencing *MICU1*, confirming the screening result (Fig. 1). We observed the same Ca^{2+} phenotype when using store-operated Ca^{2+} entry to raise intracellular free calcium31. Namely, we pre-treated cells with thapsigargin, an inhibitor of the SERCA pump, in the absence of extracellular Ca^{2+} to deplete ER stores and activate store-operated Ca^{2+} channels at the plasma membrane. The readdition of 2 mM Ca^{2+} resulted in a transient rise of $[Ca^{2+}]_m$ in control cells while *MICU1*-knockdown cells did not respond (Fig. 3b), consistent with the result obtained with histamine stimulation (Fig. 3a).

Second, we performed quantitative, single cell analyses of basal $[Ca^{2+}]_m$ and agonist-stimulated rises in $[Ca^{2+}]_m$ in HeLa cells using a mitochondria-targeted calcium FRET reporter32. We observed a significant difference in the baseline $[Ca^{2+}]_m$ in control cells versus sh1-*MICU1* knockdown cells (Table 1). Moreover, histamine treatment induced an increase in $[Ca^{2+}]_m$ in control cells (fractional saturation of 0.75 ± 0.16, n=20) that was abrogated in sh1-*MICU1* cells (fractional saturation of 0.20 ± 0.10, n=12), ($P<0.0001$). Similarly, when thapsigargin was used as calcium agonist, $[Ca^{2+}]_m$ increased in control cells (fractional saturation of 0.72 ± 0.15, n=15) but did not rise in *MICU1*-silenced cells (fractional saturation of 0.10 ± 0.01, n=11), ($P<0.0001$). Representative traces from individual cells are shown in Fig 3c and Fig. 3d.

Third, we measured mitochondrial Ca^{2+} uptake in digitonin-permeabilized cells. We selectively permeabilized the cell plasma membrane with a titrated amount of digitonin and monitored the clearance of exogenously added Ca^{2+} with Calcium Green-5N33 (see Methods). Clearance of exogenous Ca^{2+} is due to uptake by energized mitochondria via the classically defined uniporter, as it is fully abrogated by the ruthenium red derivative Ru-360 or uncoupler (Supplementary Fig. 2a,b), and not influenced by thapsigargin (Supplementary Fig. 2c). Although mitochondria of permeabilized control cells were capable of buffering multiple pulses of exogenously added Ca^{2+}, *MICU1* silenced cells showed an attenuated response (Fig. 3e).

Collectively, our secondary assays of mitochondrial Ca^{2+} uptake in cell populations and single cells with three different measurement techniques and two different Ca^{2+} agonists, confirm that MICU1 is required for mitochondrial Ca^{2+} uptake in HeLa cells, and that the Ca^{2+} phenotype in *MICU1* knockdown cells is independent of the Ca^{2+} agonist or the sensor used for detection. Moreover, MICU1 appears to have a very specific role in mitochondrial Ca^{2+} handling, since resting $[Ca^{2+}]_{ER}$, $[Ca^{2+}]_{c}$, and store-operated calcium (SOC) entry rates are not significantly different between control and knockdown cells (Table 1).

MICU1 localization and domain structure

MICU1 was first identified as a 54 kDa autoantigen34, and proteomics studies from our group and others established its mitochondrial-localization in 13 different mammalian tissues27,35. We confirmed that MICU1 localizes predominantly to mitochondria, since a carboxy-terminus GFP-tagged MICU1 exhibited clear overlap with a mitochondrial marker (Fig. 4a), with a correlation of 0.80 between red and green channels. We obtained similar results using a V5 epitope tag or other mitochondrial markers (MitoTracker Red, Mito-HcRed) (data not shown). V5-tagged MICU1 showed progressive enrichment from crude and Percoll purified mitochondria to mitoplasts prepared from HEK293 cells (Fig. 4b), consistent with a proteomic study that localized MICU1 to the inner membrane fractions of liver mitochondria29.

MICU1 has two canonical EF hands (EF1 and EF2) that are separated by an unusually long predicted helix (Fig. 4c). The two canonical EF hands are highly conserved in fish, flies, worms, and kinetoplastids, even at the level of individual residues that coordinate binding to Ca^{2+}. To determine if these EF hands are required for MICU1-mediated Ca^{2+} uptake, we created an EF mutant cell line (*MICU1*mEF). We used the sh1-insensitive cDNA construct described above (Fig. 1c) and introduced point mutations into EF1 (D231A, E242K) as well as EF2 (D421A, E432K). Although the RNAi Ca^{2+} uptake phenotype can be fully rescued by overexpression of a wild-type allele, *MICU1*mEF fails to fully restore mitochondrial calcium uptake (Fig. 4d,e). These results demonstrate that EF hands in MICU1 are essential for mitochondrial Ca^{2+} uptake.

Role of MICU1 in metabolic coupling

Several TCA cycle dehydrogenases are known to be regulated by calcium 9,10, and conversely, studies have shown that mitochondria can shape cytosolic Ca^{2+} dynamics by buffering of intracellular free calcium6,7. Such “coupling” by Ca^{2+} has been proposed to be

an important mechanism for the regulation of Ca^{2+} signaling by the mitochondrion, as well as for balancing cytosolic ATP utilization with mitochondrial ATP production36,37. We were interested in determining whether MICU1 contributes to metabolic coupling.

First, we used a cytosolic-targeted cameleon32 and monitored $[Ca^{2+}]_c$ rise in single cells challenged with thapsigargin. As illustrated in Fig. 5a and 5b, both *MICU1*-knockdown and control cells responded to calcium agonists and substantially increased their $[Ca^{2+}]_c$. However, silencing of *MICU1* slowed the clearance kinetics of $[Ca^{2+}]_c$ in response to thapsigargin (53% clearance at 200s in control cells, n=14, versus 28% clearance in *MICU1*-silenced cells, n=16, $P<0.0001$) as well as in response to histamine (representative traces shown in Fig. 5b).

Next we sought to determine whether silencing of *MICU1* can compromise the ability of cytosolic Ca^{2+} rises to simulate mitochondrial oxidative metabolism. We followed the activation of mitochondrial dehydrogenases after histamine stimulation by monitoring the level of NADH fluorescence in single cells (see Methods). As expected, NADH fluorescence increased upon challenge with rotenone and dropped following treatment with CCCP, indicating that the observed signal derived from a mitochondrial NADH pool (Supplementary Fig. 3). Treatment of control cells with histamine led to a pronounced increase in NADH (Fig. 5c), but this rise was significantly attenuated in *MICU1* silenced cells. Specifically, the histamine-induced elevation in NADH fluorescence was 117 ± 35 (n=12) in control cells versus 58 ± 28 (n=24) for *MICU1*-silenced cells ($P=3.0\times10^{-6}$). Notably, control and knockdown cell lines showed a robust elevation in NADH levels in response to rotenone treatment, suggesting that their mitochondrial NADH pools were intact.

Our studies (Fig. 5) offer strong genetic support for a role of MICU1 in coupling cytosolic Ca^{2+} transients and mitochondrial energy metabolism.

Discussion

Membrane potential-dependent uptake of Ca^{2+} by isolated mitochondria was first documented nearly 50 years ago1,2. Since then its biophysical properties have been extensively characterized13,14 but to date, none of the molecular components of this high capacity uptake machinery have been identified. Evaluating the contribution of mitochondrial Ca^{2+} uptake to intact cell physiology, growth, and development has been hampered by the lack of specific and direct inhibitors19. Our focused-RNAi screen identifies MICU1 as a key regulator of mitochondrial Ca^{2+} uptake and highlights the power of coupling integrative genomics, RNAi, and physiology. Although several mitochondrial calcium uptake mechanisms may exist15,20, our experimental data are consistent with a key role for MICU1 in regulating the classically defined uniporter. MICU1 localizes to mitochondria and its loss impairs mitochondrial Ca^{2+} uptake, in a manner that is dependent on its EF-hands, without abrogating mitochondrial respiration or membrane potential. Identification of MICU1 has allowed us to use genetics to evaluate the contribution of mitochondrial Ca^{2+} uptake to “metabolic coupling,” which has not been possible previously.

At present the precise molecular mechanism by which MICU1 controls mitochondrial Ca^{2+} uptake is not clear, but several possibilities exist: (i) MICU1 could constitute a pore-forming channel subunit, though it is unlikely to operate alone as a monomer in this capacity since it has at most one predicted membrane-spanning domain; (ii) it could be involved in buffering mitochondrial Ca^{2+} with a secondary impact on uptake, though this seems unlikely given that loss of *MICU1* expression results in reduced matrix free Ca^{2+} (Table 1); (iii) it could act as calcium sensor via its two canonical EF hands, and gate the activity of a partner channel. The latter hypothesis would be consistent with the longstanding observation that mitochondrial Ca^{2+} uniport is allosterically controlled by Ca^{2+} with a Hill coefficient of two38,39,40. Under this model, MICU1 would be functioning in a way that is similar to what has been reported for STIM1, an EF-hand-containing protein that regulates ORAI1, a store operated channel subunit41.

Future experiments will be required to determine the precise molecular mechanism by which MICU1 controls mitochondrial Ca^{2+} entry. Since our work has focused only on a single cell type, it will also be important to determine whether MICU1 plays a similar role in other cell types, or if redundant or alternate mechanisms are in place to confer tissue-specific control calcium homeostasis42,43. Regardless, the identification of MICU1 should facilitate the full molecular characterization of the mitochondrial Ca^{2+} uptake machinery, and importantly, paves the path for rigorously understanding and targeting mitochondrial Ca^{2+} uptake in normal physiology and disease.

METHODS SUMMARY

Candidate human genes required for mitochondrial Ca^{2+} uptake were prioritized based on the expression of their homologues across mouse tissues27, localization to the inner mitochondrial membrane28,29, and evolutionary conservation in kinetoplastids22,23,24 but not in yeast22,25,26. A focused RNAi screen was performed against 13 human genes in a commercially available, HeLa cell line expressing mitochondrial aequorin (mt-AEQ, Aequotech Catalog No. AT-002-H) using lentiviral constructs available from the Broad Institute's RNAi Consortium44. To rescue the *MICU1* RNAi Ca^{2+} phenotype, we custom synthesized a cDNA containing synonymous mutations at all 8 codons complementary to the strongest hairpin (Blue Heron Biotechnology). Agonist-induced rises in mitochondrial Ca^{2+} were measured in mt-AEQ HeLa cells by luminescence30,31. Measurements of Ca^{2+} uptake in permeabilized HeLa cells were made using Calcium Green 5N33. FRET based measurements of mitochondrial, cytosolic, and ER Ca^{2+} in single HeLa cells were performed using the 4mtD3cpv, D3cpv, and D1ER FRET sensors, respectively 32. Mitochondrial respiration, morphology, and mtDNA copy number were measured as previously described45. Mitochondrial membrane potential was measured by flow cytometry on cells stained with JC-1 according to manufacturer's protocol. Single cell measurements of NADH were performed via established protocols46. Crude mitochondria, Percoll purified mitochondria and mitoplasts were prepared from cultured HEK293 cells expressing MICU1-V5 as previously described47,48. Unless otherwise indicated, data are summarized as mean+/−standard deviation, and P-values correspond to t-tests.

METHODS

Prioritization of candidate genes

We used previously published datasets to prioritize candidate genes that are required for mitochondrial Ca^{2+} uptake27,28,29. We find that 18 human genes (*SQRDL, CBARA1/MICU1, GPAM, HADH, NDUFV1, NDUFA9, STOML2, NDUFA13, DCI, NDUFB9, NDUFS7, ACADL, ACADM, ACADVL, OXCT1, NDUFV2, PTGES2, NDUFS1*) meet the requirements for (i) a reliable mitochondrial localization based on our previously published MitoCarta inventory of 1098 mouse mitochondrial proteins27 (1013 human homologues) (www.broad.mit.edu/publications/MitoCarta), (ii) association with the mitochondrial inner membrane based on proteomic studies of mouse and rat liver mitochondria28,29 (225/1013), (iii) evolutionary conservation in kinetoplastids but not in yeast (58/1013) according to our previously published phylogenetic analysis27 and (iv) protein expression across at least 10 mouse tissues (616/1013) based on our mitochondrial tissues atlas27. Of these, 5 genes (*ACADL, ACADM, ACADVL, OXCT1, PTGES2*) had obvious roles in other pathways or RNAi reagents were not available and were therefore not pursued.

Cell culture

HeLa cells expressing a commercially available mitochondrial matrix targeted aequorin (mt-AEQ) (Aequotech Catalog No. AT-002-H) were grown in DMEM High glucose medium (Invitrogen Cat No. 11995) with 10% FBS (Gibco Cat No. 16000) and 100 μg/ml geneticin (Gibco Cat No. 10131-035) at 37°C and 5% CO_2. mt-AEQ HeLa cells expressing gene-specific lentiviral shRNAs were grown in selective medium containing DMEM High glucose medium, 10% FBS, 100 μg/ml geneticin and 2 μg/ml puromycicn (Sigma Cat No. P9620).

RNA interference screen

A shRNA library of lentiviral particles targeting our 13 candidate genes and containing shRNA positive controls were purchased from the Broad Institute's RNAi Consortium and arrayed in one 96-well plate. Two independent screens were performed. Briefly, 15K mt-AEQ HeLa cells were seeded in a 96-well plate (PerkinElmer Cat No. 6005181). After 12 hr the medium was replaced with DMEM High glucose medium supplemented with 10% FBS and 8 μg/ml polybrene (Sigma Cat No. H9268). Infection was performed by addition of 60 μl of gene specific shRNA lentivirus to each well followed by a 30 min spin at 800rcf at 37°C. Cells were washed three times with regular growth media and returned to 37°C at 5% CO_2. 24 hr post-infection, infected cells were selected in growth media supplemented with 2 μg/ml puromycin. Luminescence-based measurements of mitochondrial Ca^{2+} and cell number were performed 6 days post-infection. Cell number and viability were assayed by CellTiter-Glo Luminescent Viability assay (Promega Cat No. G7571).

cDNA rescue experiments

A version of *MICU1* cDNA resistant to sh1-*MICU1* knock-down was de novo synthesized and cloned into pENTR221 vector, ready for use in the Gateway Technology System (Blue Heron Biotechnology). The cDNA harboured 8 synonymous mutations in the codons

complementary to sh1-*MICU1*. Similarly, a mutated version of sh1-*MICU1* insensitive cDNA was de novo synthesized which harbors two point mutations into the first EF hand domain, EF1 (D231A, E242K) as well as two mutations in the second EF hand domain, EF2 (D421A, E432K) to create a *MICU1* EF mutant (*MICU*mEF). Procedures and reagents for virus production and infection have been previously published44. 24 h postinfection sh1-*MICU1* knockdown cells expressing sh1-*MICU1* resistant cDNAs were selected with 2 μg/ml puromycin (Sigma #P9620) and 10 μg/ml blasticidin (Invitrogen # A11139).

Luminescence-based measurement of mitochondrial Ca^{2+}

Measurements of mitochondrial Ca^{2+} were performed upon both histamine and thapsigargin treatment as reported in Brini *et al.* and Glitsch *et al*30,31. In all cases light emission was measured in a luminescence counter (MicroBeta2 LumiJET Microplate Counter PerkinElmer) at 469nm every 0.1 sec.

Assays of mitochondrial membrane potential, respiration and mtDNA abundance

Mitochondrial respiration and mtDNA copy number were measured as previously described 45. Mitochondrial membrane potential was measured by flow cytometry (BD Biosciences LSR II flow cytometer) using cells stained with JC-1 according to manufacturer's protocol. JC-1 was excited at 488nm, green fluorescence quantified between 515 and 545nm, and red fluorescence quantified between 562 and 588nm.

Measurement of mitochondrial Ca^{2+} uptake in digitonin-permeabilized cells

Extramitochondrial free Ca^{2+} was monitored in the presence of digitonin-permeabilized cells as described in Murphy *et al*33. Briefly, cells (2×10^6 cells/ml) were resuspended in KCl medium (125 mM KCl, 2 mM K_2HPO_4, 1 mM $MgCl_2$, 20 mM Hepes, pH 7.0) containing 5 mM glutamate, 5 mM malate and 5 mM succinate as oxidable substrates and 0.5 uM Ca^{2+} green-5N. The plasma membranes were then selectively permeabilized with digitonin (0.01%wt/vol final). Fluorescence (Ex506/Em531 nm) was monitored at 27°C using a Perkin-Elmer LS-50B fluorescence spectrophotometer equipped with a stirring device.

FRET based measurement of mitochondrial, cytosolic, and ER Ca^{2+}

Cytosolic, mitochondrial, and ER Ca^{2+} levels were measured using the D3cpv, 4mtD3cpv, and D1ER Ca^{2+} sensors, respectively32. Details on these sensors have been published previously5,49. Briefly, cells were seeded on 3.5 cm imaging dishes, transiently transfected using TransIt (Mirus) according to manufacturer's protocol, and were imaged 48 hours after transfection. Imaging experiments were performed on an Axiovert 200M inverted fluorescence microscope (Zeiss) with a Cascade 512B CCD camera (Roper scientific), and equipped with CFP (430/24 excitation, 455 dichroic, 470/24 emission), YFP (495/10 excitation, 515 dichroic, 535/25 emission) and FRET (430/24 excitation, 455 dichroic, 535/25 emission) filters controlled by a Lambda 10-3 filter changer (Sutter Instruments) and analyzed using Metafluor software (Universal Imaging). Details on the microscope, sensor calibration, and conversion of FRET ratios (including protocol for obtaining R_{min} and R_{max})

into Ca^{2+} concentrations have been published32. Statistical significance was evaluated using either Student's t-test or two sample ANOVA.

Microscopy-based NADH measurements

Measurement of cellular NADH was carried out according to established protocols46. Briefly, cells were treated with histamine (150 μM), followed by rotenone (2 μM). The NADH signal was measured with the following settings: 380/10 excitation filter, 455 dichroic, 475/24 emission filter, and 0.6 (25% transmission) neutral density filter, and 1000 ms exposure time.

Isolation of mitochondria and Western blot analysis

Cell lysates, crude and Percoll purified mitochondria were prepared from cultured HEK293 cells47. Percoll purified mitochondria (0.2 mg) were hypotonically lysed as previously described48. Immunoblotting of the four fractions (5 ug) was performed with commercially available antibodies: anti-cytochrome *c* (Mitoscience #MSA06), anti-ATP synthase subunit alpha (Mitoscience, #MS502) and anti-V5 antibody (Invitrogen, R96025).

Supplementary Material

Refer to Web version on PubMed Central for supplementary material.

Acknowledgements

We thank Z. Grabarek, S. Silver, and D. Root for valuable discussions; S. Calvo for assistance with bioinformatics; Panfilo Federico for technical assistance; and members of the Mootha Laboratory for valuable feedback. This work was supported by grants from the National Institutes of Health (GM084027) to A.E.P, (TR2 GM08759) to J.M, and (GM0077465, DK080261) awarded to V.K.M. and by an HHMI Early Career Physician Scientist Award to V.K.M.

REFERENCES

1. Deluca HF, Engstrom GW. Calcium uptake by rat kidney mitochondria. Proc Natl Acad Sci U S A. 1961; 47:1744–1750. [PubMed: 13885269]
2. Vasington FD, Murphy JV. Ca ion uptake by rat kidney mitochondria and its dependence on respiration and phosphorylation. J Biol Chem. 1962; 237:2670–2677. [PubMed: 13925019]
3. Rizzuto R, Simpson AW, Brini M, Pozzan T. Rapid changes of mitochondrial Ca2+ revealed by specifically targeted recombinant aequorin. Nature. 1992; 358:325–327. [PubMed: 1322496]
4. Filippin L, Magalhaes PJ, Di Benedetto G, Colella M, Pozzan T. Stable interactions between mitochondria and endoplasmic reticulum allow rapid accumulation of calcium in a subpopulation of mitochondria. J Biol Chem. 2003; 278:39224–39234. [PubMed: 12874292]
5. Palmer AE, et al. Ca2+ indicators based on computationally redesigned calmodulin-peptide pairs. Chem Biol. 2006; 13:521–530. [PubMed: 16720273]
6. Jouaville LS, Ichas F, Holmuhamedov EL, Camacho P, Lechleiter JD. Synchronization of calcium waves by mitochondrial substrates in Xenopus laevis oocytes. Nature. 1995; 377:438–441. [PubMed: 7566122]
7. Kaftan EJ, Xu T, Abercrombie RF, Hille B. Mitochondria shape hormonally induced cytoplasmic calcium oscillations and modulate exocytosis. J Biol Chem. 2000; 275:25465–25470. [PubMed: 10835418]
8. Spat A, Szanda G, Csordas G, Hajnoczky G. High- and low-calcium-dependent mechanisms of mitochondrial calcium signalling. Cell Calcium. 2008; 44:51–63. [PubMed: 18242694]

9. Denton RM, McCormack JG. The role of calcium in the regulation of mitochondrial metabolism. Biochem Soc Trans. 1980; 8:266–268. [PubMed: 7399049]
10. Hajnoczky G, Robb-Gaspers LD, Seitz MB, Thomas AP. Decoding of cytosolic calcium oscillations in the mitochondria. Cell. 1995; 82:415–424. [PubMed: 7634331]
11. Balaban RS. The role of Ca(2+) signaling in the coordination of mitochondrial ATP production with cardiac work. Biochim Biophys Acta. 2009; 1787:1334–1341. [PubMed: 19481532]
12. Bernardi P, Rasola A. Calcium and cell death: the mitochondrial connection. Subcell Biochem. 2007; 45:481–506. [PubMed: 18193649]
13. Gunter KK, Gunter TE. Transport of calcium by mitochondria. J Bioenerg Biomembr. 1994; 26:471–485. [PubMed: 7896763]
14. Kirichok Y, Krapivinsky G, Clapham DE. The mitochondrial calcium uniporter is a highly selective ion channel. Nature. 2004; 427:360–364. [PubMed: 14737170]
15. Santo-Domingo J, Demaurex N. Calcium uptake mechanisms of mitochondria. Biochim Biophys Acta. 2010; 1797:907–912. [PubMed: 20079335]
16. Mironova GD, et al. Isolation and properties of Ca2+-transporting glycoprotein and peptide from beef heart mitochondria. J Bioenerg Biomembr. 1982; 14:213–225. [PubMed: 7130161]
17. Panfili E, et al. Specific inhibition of mitochondrial Ca2+ transport by antibodies directed to the Ca2+-binding glycoprotein. Nature. 1976; 264:185–186. [PubMed: 995204]
18. Zazueta C, Zafra G, Vera G, Sanchez C, Chavez E. Advances in the purification of the mitochondrial Ca2+ uniporter using the labeled inhibitor 103Ru360. J Bioenerg Biomembr. 1998; 30:489–498. [PubMed: 9932651]
19. Hajnoczky G, et al. Mitochondrial calcium signalling and cell death: approaches for assessing the role of mitochondrial Ca2+ uptake in apoptosis. Cell Calcium. 2006; 40:553–560. [PubMed: 17074387]
20. Sparagna GC, Gunter KK, Sheu SS, Gunter TE. Mitochondrial calcium uptake from physiological-type pulses of calcium. A description of the rapid uptake mode. J Biol Chem. 1995; 270:27510–27515. [PubMed: 7499209]
21. Jiang D, Zhao L, Clapham DE. Genome-wide RNAi screen identifies Letm1 as a mitochondrial Ca2+/H+ antiporter. Science. 2009; 326:144–147. [PubMed: 19797662]
22. Carafoli E, Lehninger AL. A survey of the interaction of calcium ions with mitochondria from different tissues and species. Biochem J. 1971; 122:681–690. [PubMed: 5129264]
23. Docampo R, Vercesi AE. Ca2+ transport by coupled Trypanosoma cruzi mitochondria in situ. J Biol Chem. 1989; 264:108–111. [PubMed: 2491844]
24. Vercesi AE, Docampo R. Ca2+ transport by digitonin-permeabilized Leishmania donovani. Effects of Ca2+, pentamidine and WR-6026 on mitochondrial membrane potential in situ. Biochem J. 1992; 284(Pt 2):463–467. [PubMed: 1376113]
25. Balcavage WX, Lloyd JL, Mattoon JR, Ohnishi T, Scarpa A. Cation movements and respiratory response in yeast mitochondria treated with high Ca2+ concentrations. Biochim Biophys Acta. 1973; 305:41–51. [PubMed: 4578276]
26. Uribe S, Rangel P, Pardo JP. Interactions of calcium with yeast mitochondria. Cell Calcium. 1992; 13:211–217. [PubMed: 1586938]
27. Pagliarini DJ, et al. A mitochondrial protein compendium elucidates complex I disease biology. Cell. 2008; 134:112–123. [PubMed: 18614015]
28. Da Cruz S, et al. Proteomic analysis of the mouse liver mitochondrial inner membrane. J Biol Chem. 2003; 278:41566–41571. [PubMed: 12865426]
29. McDonald T, et al. Expanding the subproteome of the inner mitochondria using protein separation technologies: one- and two-dimensional liquid chromatography and two-dimensional gel electrophoresis. Mol Cell Proteomics. 2006; 5:2392–2411. [PubMed: 17000643]
30. Brini M, Pinton P, Pozzan T, Rizzuto R. Targeted recombinant aequorins: tools for monitoring [Ca2+] in the various compartments of a living cell. Microsc Res Tech. 1999; 46:380–389. [PubMed: 10504215]
31. Glitsch MD, Bakowski D, Parekh AB. Store-operated Ca2+ entry depends on mitochondrial Ca2+ uptake. Embo J. 2002; 21:6744–6754. [PubMed: 12485995]

32. Palmer AE, Tsien RY. Measuring calcium signaling using genetically targetable fluorescent indicators. Nat Protoc. 2006; 1:1057–1065. [PubMed: 17406387]
33. Murphy AN, Bredesen DE, Cortopassi G, Wang E, Fiskum G. Bcl-2 potentiates the maximal calcium uptake capacity of neural cell mitochondria. Proc Natl Acad Sci U S A. 1996; 93:9893–9898. [PubMed: 8790427]
34. Aichberger KJ, et al. Hom s 4, an IgE-reactive autoantigen belonging to a new subfamily of calcium-binding proteins, can induce Th cell type 1-mediated autoreactivity. J Immunol. 2005; 175:1286–1294. [PubMed: 16002733]
35. Forner F, et al. Proteome differences between brown and white fat mitochondria reveal specialized metabolic functions. Cell Metab. 2009; 10:324–335. [PubMed: 19808025]
36. Jouaville LS, Pinton P, Bastianutto C, Rutter GA, Rizzuto R. Regulation of mitochondrial ATP synthesis by calcium: evidence for a long-term metabolic priming. Proc Natl Acad Sci U S A. 1999; 96:13807–13812. [PubMed: 10570154]
37. Territo PR, Mootha VK, French SA, Balaban RS. Ca(2+) activation of heart mitochondrial oxidative phosphorylation: role of the F(0)/F(1)-ATPase. Am J Physiol Cell Physiol. 2000; 278:C423–C435. [PubMed: 10666039]
38. Bragadin M, Pozzan T, Azzone GF. Kinetics of Ca2+ carrier in rat liver mitochondria. Biochemistry. 1979; 18:5972–5978. [PubMed: 42437]
39. Igbavboa U, Pfeiffer DR. EGTA inhibits reverse uniport-dependent Ca2+ release from uncoupled mitochondria. Possible regulation of the Ca2+ uniporter by a Ca2+ binding site on the cytoplasmic side of the inner membrane. J Biol Chem. 1988; 263:1405–1412. [PubMed: 2447088]
40. Moreau B, Nelson C, Parekh AB. Biphasic regulation of mitochondrial Ca2+ uptake by cytosolic Ca2+ concentration. Curr Biol. 2006; 16:1672–1677. [PubMed: 16920631]
41. Zhang SL, et al. STIM1 is a Ca2+ sensor that activates CRAC channels and migrates from the Ca2+ store to the plasma membrane. Nature. 2005; 437:902–905. [PubMed: 16208375]
42. Lawrie AM, Rizzuto R, Pozzan T, Simpson AW. A role for calcium influx in the regulation of mitochondrial calcium in endothelial cells. J Biol Chem. 1996; 271:10753–10759. [PubMed: 8631885]
43. Favaron M, Bernardi P. Tissue-specific modulation of the mitochondrial calcium uniporter by magnesium ions. FEBS Lett. 1985; 183:260–264. [PubMed: 3987891]
44. Moffat J, et al. A lentiviral RNAi library for human and mouse genes applied to an arrayed viral high-content screen. Cell. 2006; 124:1283–1298. [PubMed: 16564017]
45. Gohil VM, et al. Nutrient-sensitized screening for drugs that shift energy metabolism from mitochondrial respiration to glycolysis. Nat Biotechnol. 2010; 28:249–255. [PubMed: 20160716]
46. Gaspers LD, Thomas AP. Calcium-dependent activation of mitochondrial metabolism in mammalian cells. Methods. 2008; 46:224–232. [PubMed: 18854213]
47. Mootha VK, et al. Integrated analysis of protein composition, tissue diversity, and gene regulation in mouse mitochondria. Cell. 2003; 115:629–640. [PubMed: 14651853]
48. Mootha VK, et al. A reversible component of mitochondrial respiratory dysfunction in apoptosis can be rescued by exogenous cytochrome c. Embo J. 2001; 20:661–671. [PubMed: 11179211]
49. Palmer AE, Jin C, Reed JC, Tsien RY. Bcl-2-mediated alterations in endoplasmic reticulum Ca2+ analyzed with an improved genetically encoded fluorescent sensor. Proc Natl Acad Sci U S A. 2004; 101:17404–17409. [PubMed: 15585581]

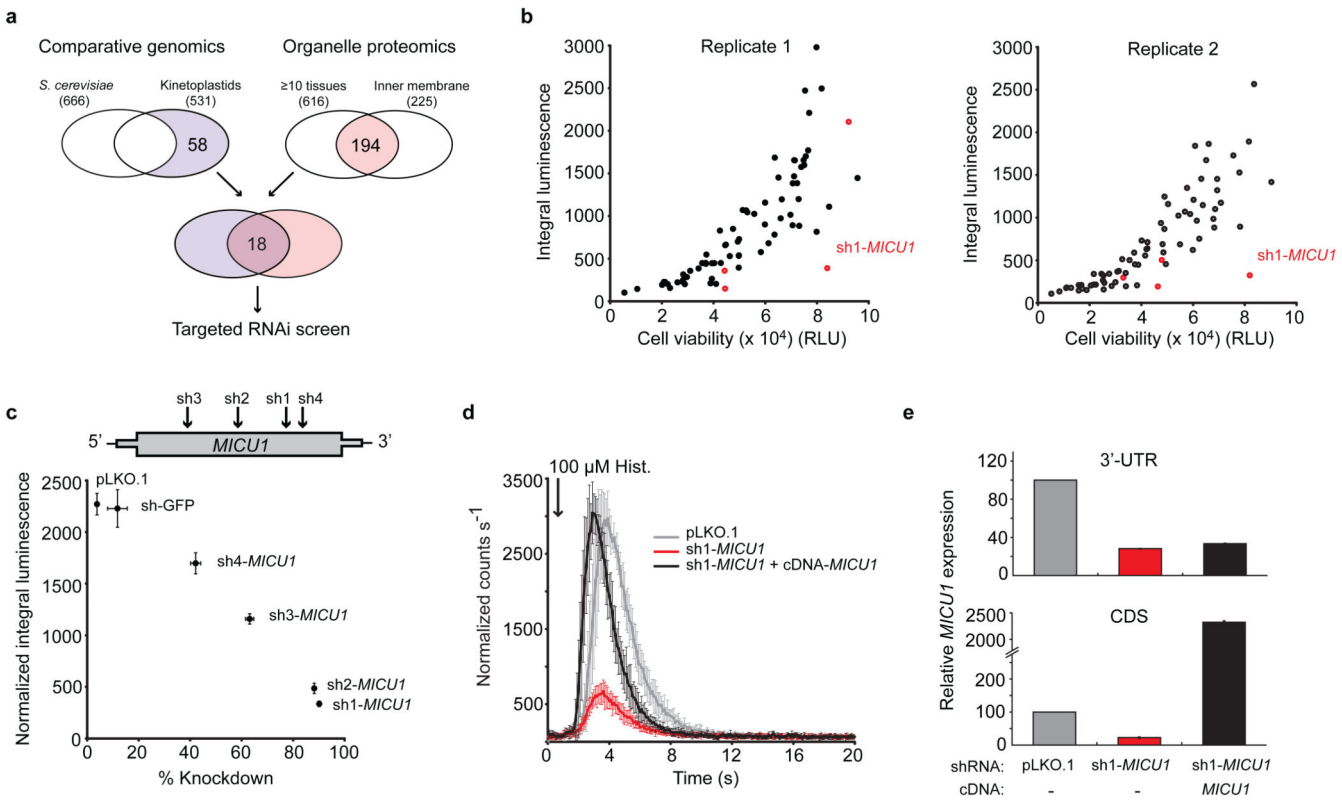

Fig. 1. Targeted RNAi screen for mitochondrial Ca^{2+} uptake

(a) Integrative approach to predict human mitochondrial proteins involved in mitochondrial Ca^{2+} uptake. Numbers represent the subset of human MitoCarta genes with the indicated property. (b) Targeted RNAi screen of mitochondrial Ca^{2+} uptake for 13 of the 18 top candidate genes. Each circle represents one RNAi hairpin expressed in mt-AEQ HeLa cells. Mitochondrial Ca^{2+} uptake, reported as the integral luminescence following 100 μM histamine stimulation, is plotted as a function of cell viability (relative luminescence units, RLU). RNAi hairpins targeting *MICU1* are shown in red. (c) Relationship between mitochondrial Ca^{2+} uptake and *MICU1* knockdown. The region of the *MICU1* cDNA targeted by four distinct hairpins (sh1–sh4) is shown. Integral luminescence normalized to cell number (mean ± s.d., n=8) is plotted as a function of relative *MICU1* gene expression using actin as an endogenous control (mean ± s.d., n=3). (d) cDNA rescue of the sh1-*MICU1* mitochondrial Ca^{2+} phenotype. Kinetic traces of mitochondrial Ca^{2+} uptake normalized to cell number are shown for control cells (pLKO.1), *MICU1*-silenced cells, and rescue cells (mean ± s.d., n=3). (e) Quantification of endogenous (3'-UTR) and endogenous + exogenous (CDS) *MICU1* expression in control, *MICU1* knockdown, and rescue cells measured by qPCR and reported as relative expression using actin as an endogenous control (mean ± s.d., n=3).

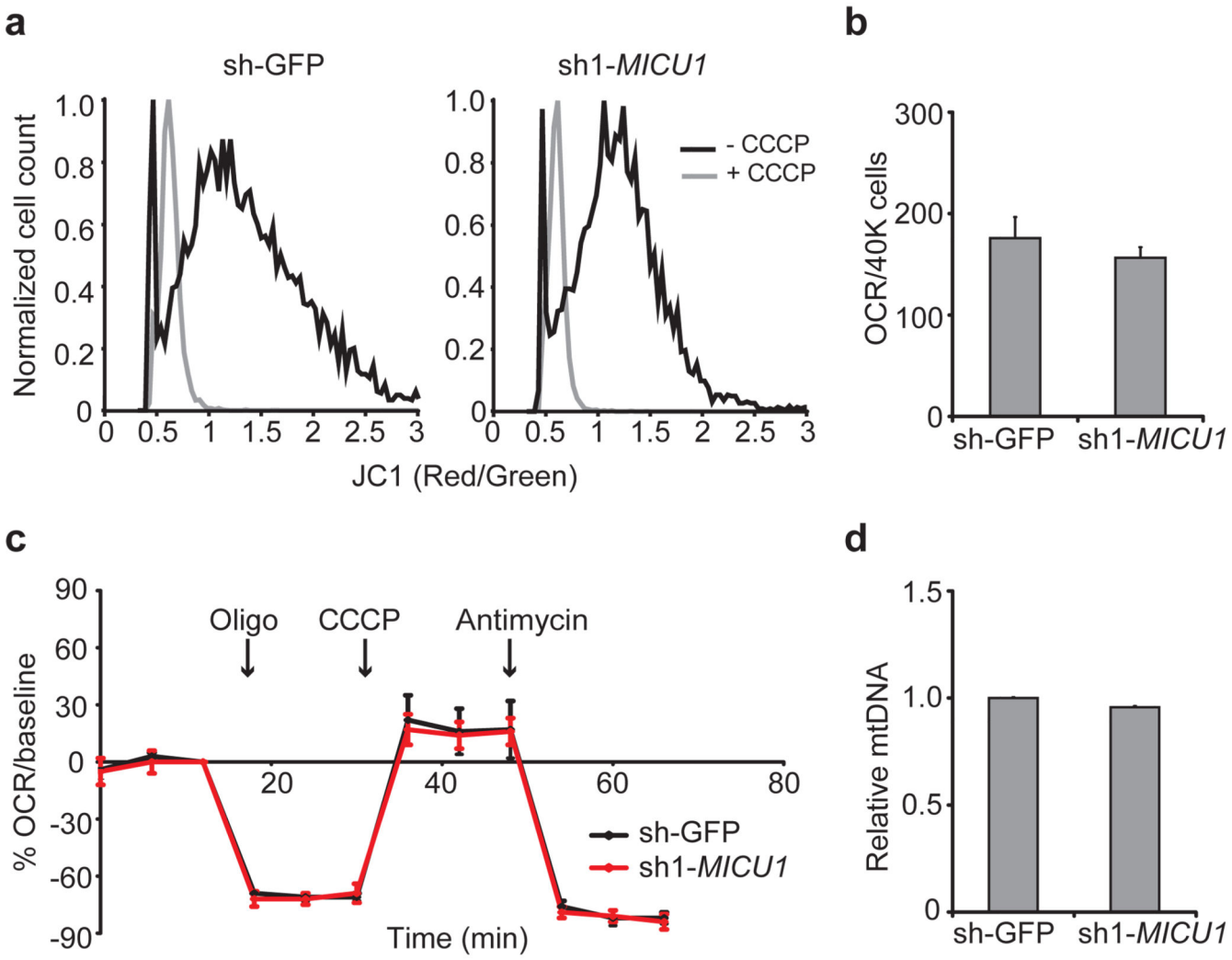

Fig. 2. Mitochondrial membrane potential, respiration, and abundance in *MICU1*-silenced cells

(a) Mitochondrial membrane potential in *MICU1*-knockdown (sh1-*MICU1*) and control (sh-*GFP*) cells measured by JC-1 fluorescence in the presence or absence of the uncoupler CCCP (5 μM). (b) Basal oxygen consumption rate (OCR, pmol O_2/min) in control and knockdown cells. (c) Normalized OCR in *MICU1*-knockdown and control cells following the addition of the complex V inhibitor oligomycin (Oligo; 0.5 μM), uncoupler CCCP (0.5 μM), and complex III inhibitor antimycin (0.5 μM). Results are mean ± s.d of five independent replicates. (d) mtDNA copy-number relative to nuclear DNA in *MICU1*-knockdown and control cells. Values are mean+/−s.d of three independent replicates.

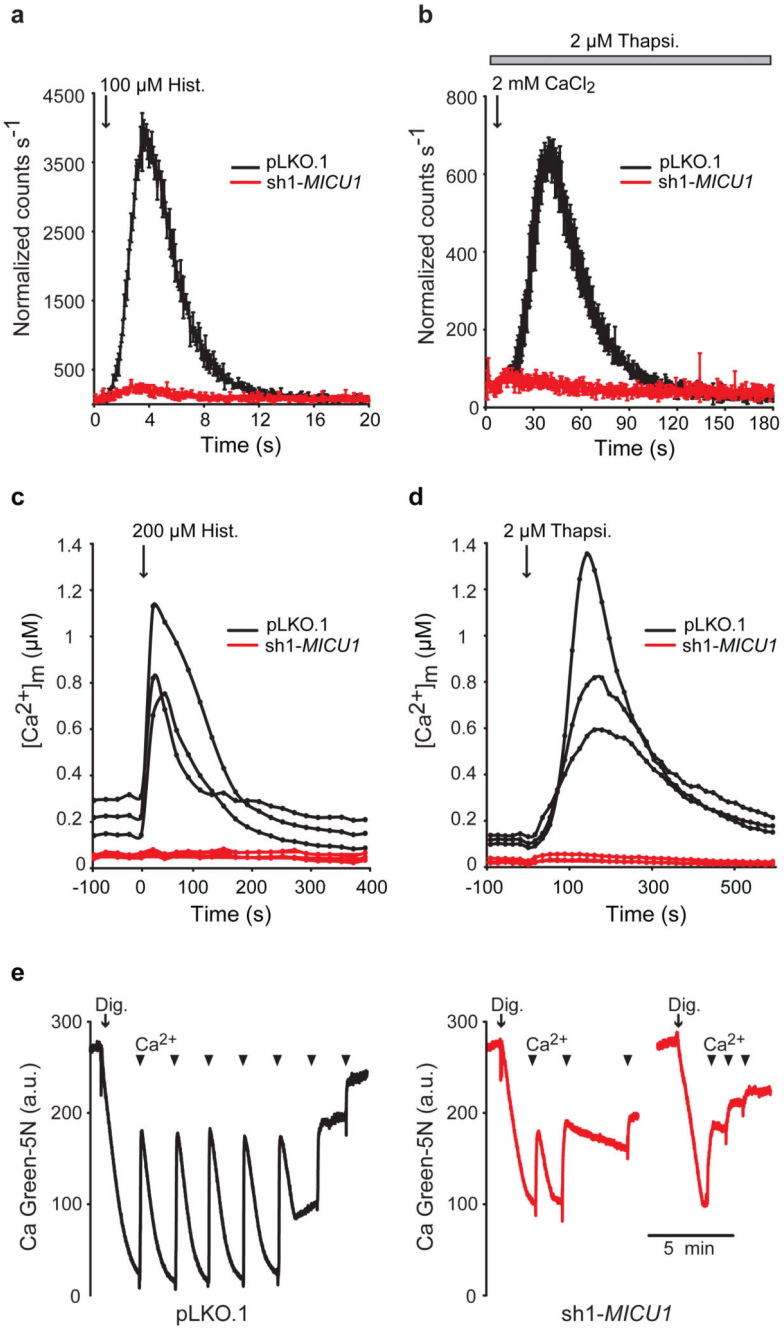

Fig. 3. Measurement of mitochondrial Ca^{2+} uptake kinetics in populations of cells, individual cells, and permeabilized cells

(a) Luminescence measurements of mitochondrial Ca^{2+} in *MICU1*-silenced (sh1-*MICU1*) and control (pLKO.1) mt-AEQ cells normalized to 30K cells (mean ± s.d., n=3). (b) Luminescence measurements of mitochondrial Ca^{2+} post addition of $CaCl_2$ in cells pre-treated with thapsigargin (mean ± s.d., n=3). (c) Representative single-cell measurements of mitochondrial Ca^{2+} dynamics in HeLa cells measured by FRET following treatment with histamine. Traces are representative of n=20 control and n=12 knockdown cells. (d) Similar

measurements in HeLa cells following stimulation with thapsigargin. Traces are representative of n=15 control and n=11 knockdown cells. (e) Representative traces of mitochondrial Ca^{2+} uptake in digitonin-permeabilized mt-AEQ HeLa cells using Calcium Green-5N (0.5 μM) to measure extramitochondrial Ca^{2+}. Arrowheads denote addition of 100 uM pulses of $CaCl_2$.

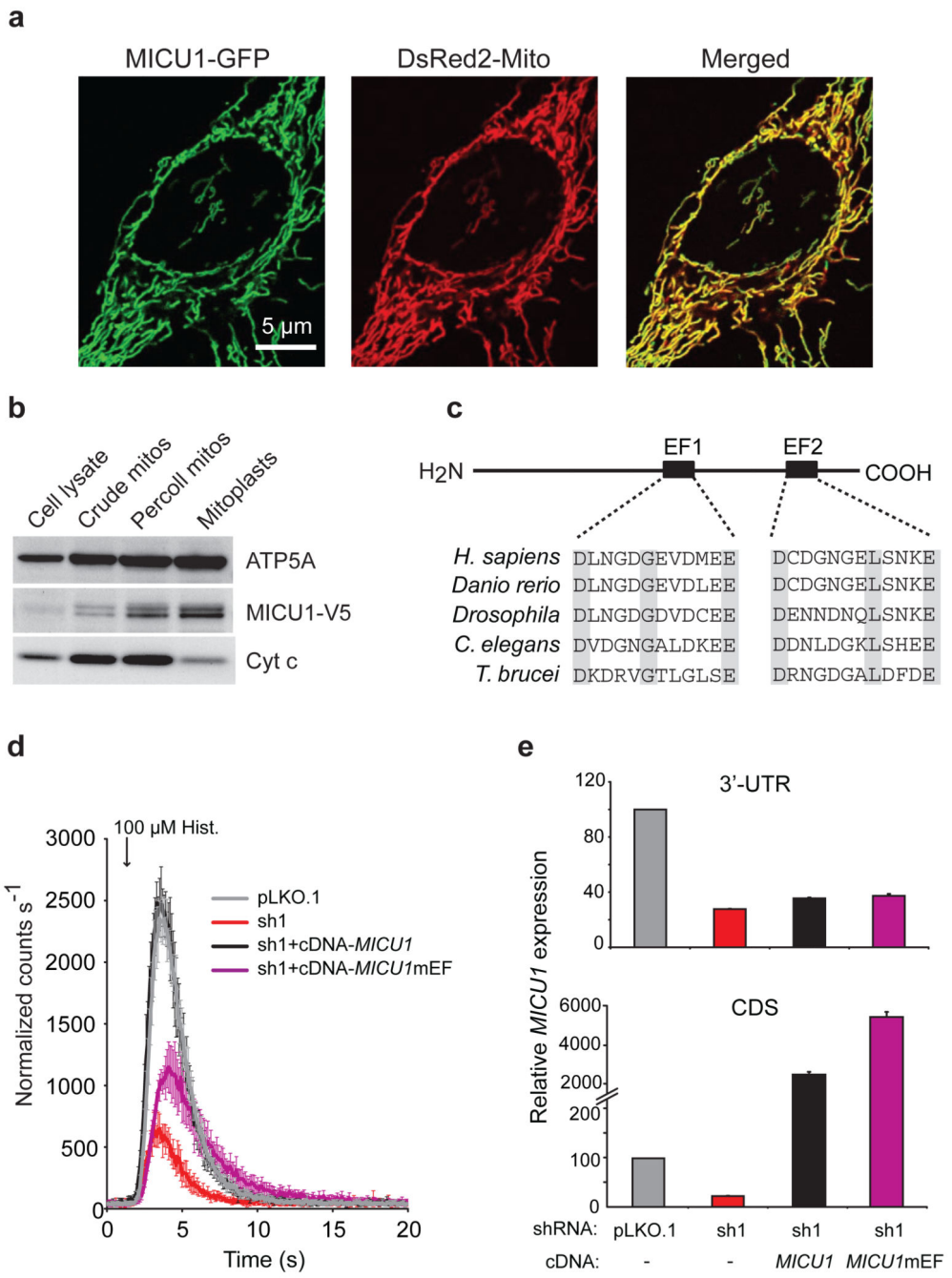

Fig. 4. MICU1 is an EF-hand protein localized to mitochondria

(a) Confocal microscopy image of a HeLa cell expressing MICU1-GFP and DsRed2-Mito. (b) Immunoblot analysis of whole cell lysates, crude mitochondria, Percoll purified mitochondria, and mitoplasts isolated from HEK293 cells expressing a COOH-terminus V5-tagged version of MICU1. (c) Domain structure of MICU1 highlighting two evolutionarily conserved EF hands. (d) cDNA rescue of the sh1-*MICU1* mitochondrial Ca^{2+} uptake phenotype using a cDNA expressing a wild-type allele of MICU1 or an EF mutant (MICU1mEF) (mean ± s.d., n=3). (e) Quantification of endogenous (3'-UTR) and

endogenous + exogenous (CDS) *MICU1* expression for the rescue experiment in (d). Relative gene expression is reported as fold change over control cells (pLKO.1) using actin as an endogenous control (mean ± s.d., n=3).

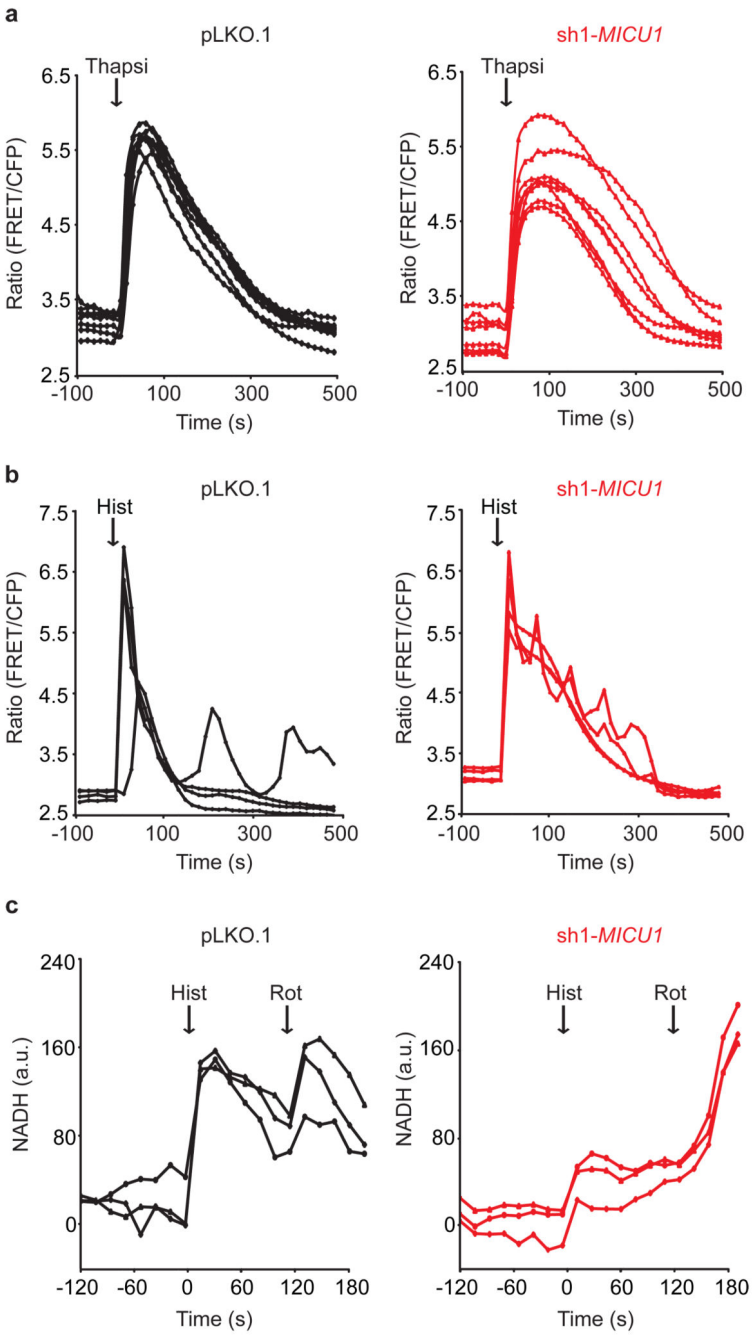

Fig. 5. Contribution of *MICU1* to cytosolic Ca^{2+} dynamics and metabolic coupling

(a) Thapsigargin (5 uM) evoked changes in cytosolic [Ca^{2+}] measured using a FRET reporter in *MICU1*-silenced (sh1-*MICU1*) and control (pLKO.1) cells and reported as a FRET ratio. Traces are representative of n=14 for control and n=16 for knockdown cells. (b) Histamine (200 uM) evoked changes in cytosolic [Ca^{2+}] in *MICU1*-silenced and control cells. Traces are representative of n=28 for control and n=17 for knockdown cells. (c) Single cell measurement of NADH in *MICU1*-silenced and control cells. Where indicated, cells are

challenged with 150 μM histamine (Hist) and 2 μM rotenone (Rot). Traces are representative of n=12 and n=24 knockdown cells.

Table 1

Intracellular Calcium Measurements

	pLKO.1	sh1-*MICU1*	*P*-value[3]
Resting $[Ca^{2+}]_m$	0.21 ± 0.08 μM (*n*=30)	0.04 μM ± 0.01 (*n*=25)	< .0001
Resting $[Ca^{2+}]_c$	0.10 ± 0.06 μM (*n*=38)	0.08 μM ± 0.06 (*n*=40)	0.10
Resting $[Ca^{2+}]_{ER}$[1]	0.69 ± 0.12 (*n*=18)	0.68 ± 0.09 (*n*=22)	0.99
SOCE amplitude[2]	0.78 ± 0.18 (*n*=21)	0.76 ± 0.08 (*n*=21)	0.67

[1] Data are reported as ΔR ($R - R_{min}$).

[2] Store Operated Calcium Entry, SOCE. Data are reported as fraction of the maximum value, $(R_{SOCE} - R_{min})/R_{max} - R_{min}$).

[3] *P*-values correspond to two-sided Student's t-test with unequal variance for resting $[Ca^{2+}]_C$, resting $[Ca^{2+}]_{ER}$, and SOCE. For resting $[Ca^{2+}]_m$, *P*-value corresponds to one-way ANOVA.